

# MEASUREMENT AND CHARACTERIZATION OF GRANULATION PATTERNS IN THE IAG SOLAR SPECTRA

---

Claudia Alejandra Cuellar Nieto

Benjamin Oostra Vannopen

Final project

# MOTIVATION

- \* For decades, the solar spectrum has served as the fundamental reference point for spectroscopic analysis by using disk-integrated flux spectra.
- \* Advances in optical instrumentation have recently providing new insights into solar properties from dynamics to surface geometry. A key example of this is the solar granulation pattern and line-depth-dependence of the convective blueshift.

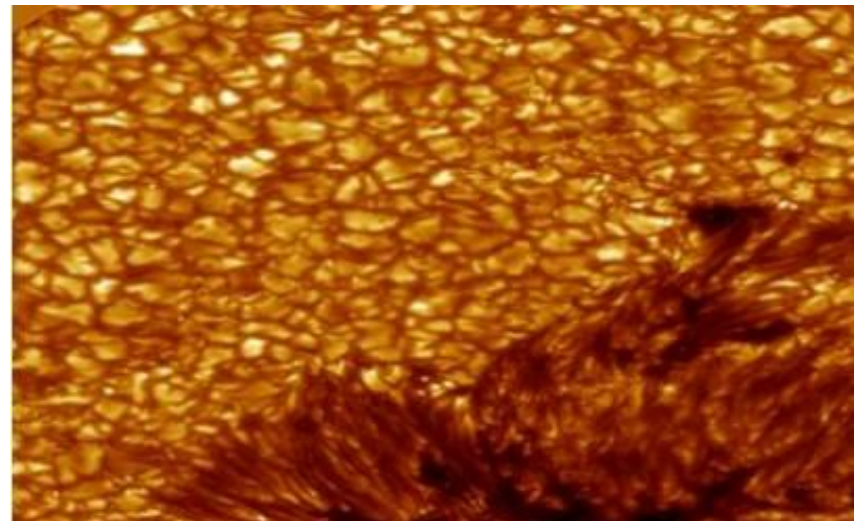


Figure 1: A view of the granulation pattern on the Sun's surface. Image taken from [1].

Our approach involves measuring the granulation pattern using the IAG Solar Flux Atlas. Published by Reiners et al. in 2016 [2], this atlas provides highly precise and accurate data, with radial velocity uncertainties on the order of  $\pm 10$  m/s across the wavelength range of 4050 to 10650 Å.

- \* We aim to establish a characterization to line depth of the granulation pattern by treating the sun as any other star.
- \* Since we are working with the Sun's spectrum, we must account for the specific signatures of its hydrodynamics. These effects can be summarized through three signatures: Line broadening, line bisector asymmetry, and line depth dependence.

---

[2] A. Reiners, N. Mrotzek, U. Lemke, J. Hinrichs, and K. Reinsch, The IAG solar flux atlas: Accurate wavelengths and absolute convective blueshift in standard solar spectra, *A&A* 587, A65 (2016).

# THE IAG SOLAR FLUX ATLAS

In 2016 Reiners observed and published the Solar Flux Atlas with an FTS Spectrograph at the *Institut für Astrophysik, Göttingen* (IAG).

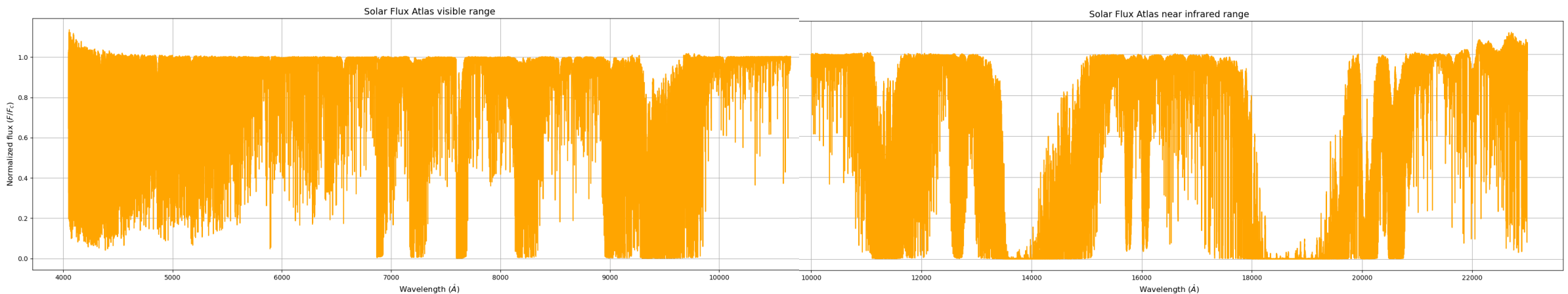


Figure 2: Solar Flux Atlas graph for normalized flux against wavelength.

He and collaborators showed that is the most precise and accurate Solar Flux Atlas currently available. In contrast to other FTS atlases, the entire visible wavelength range was observed simultaneously using only one spectrograph setting [2].

---

[2] A. Reiners, N. Mrotzek, U. Lemke, J. Hinrichs, and K. Reinsch, The IAG solar flux atlas: Accurate wavelengths and absolute convective blueshift in standard solar spectra, *A&A* 587, A65 (2016).

# THE IAG SPATIALLY RESOLVED QUIET SUN ATLAS

In 2023 Ellwarth et al. observed and published the Spatially Resolved Quiet Sun Atlas with an FTS Spectrograph at *the Institut für Astrophysik, Göttingen* (IAG).

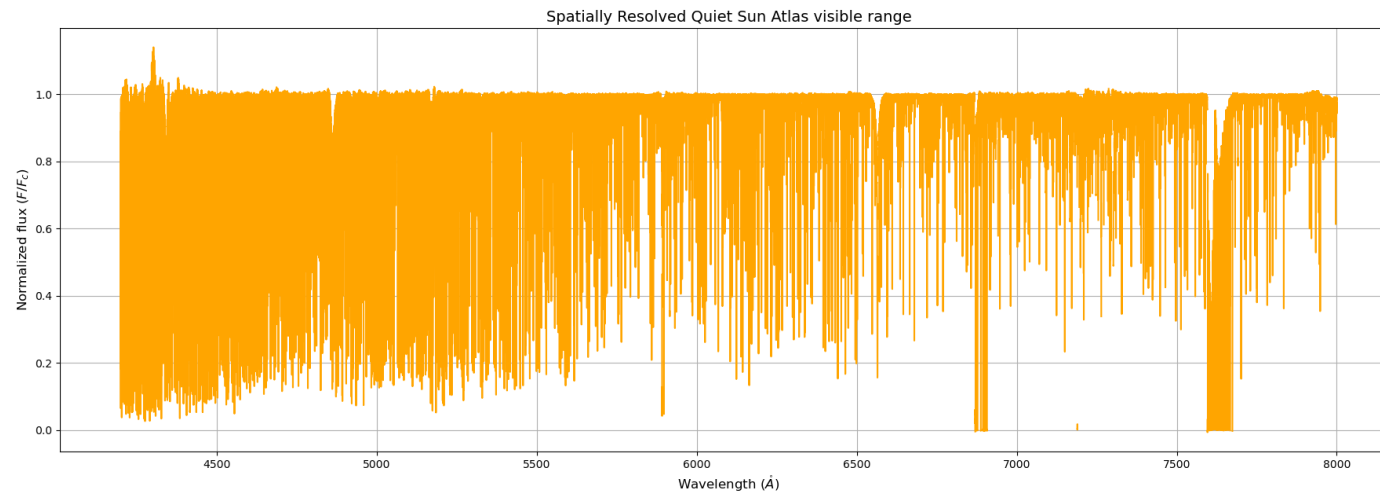


Figure 3: Spatially Resolved Quiet Sun Atlas graph for normalized flux against wavelength.

He and collaborators used observations from the disc center ( $\mu = 1.0$ ) towards the solar limb ( $\mu = 0$ ), where  $\mu = \cos(\theta)$  [3].

---

[3] M. Ellwarth, B. Ehmann, S. Schäfer, and A. Reiners, Convective characteristics of Fe I lines across the solar disc, *A&A* 680, A62 (2023).

# WHY USE TWO DIFFERENT SPECTRAL DATASETS?

- \* Our principal objective is to establish a characterization of the granulation pattern by treating the Sun as a star. This approach allows us to develop methods that can be directly scaled and applied to other solar-type stars.
- \* To accurately analyze relative velocities and dynamics, we must account for insights that can only be corrected using the Spatially Resolved Quiet Sun Atlas.

# WHAT IS THE SOLAR GRANULATION PATTERN?

- \* The granulation pattern is revealed in a graph of convective blueshift against line depth, which clearly illustrates the convective motion of the photosphere.
- \* This phenomenon has been particularly documented by David Gray. His research has significantly improved the precision of stellar radial velocity measurements.

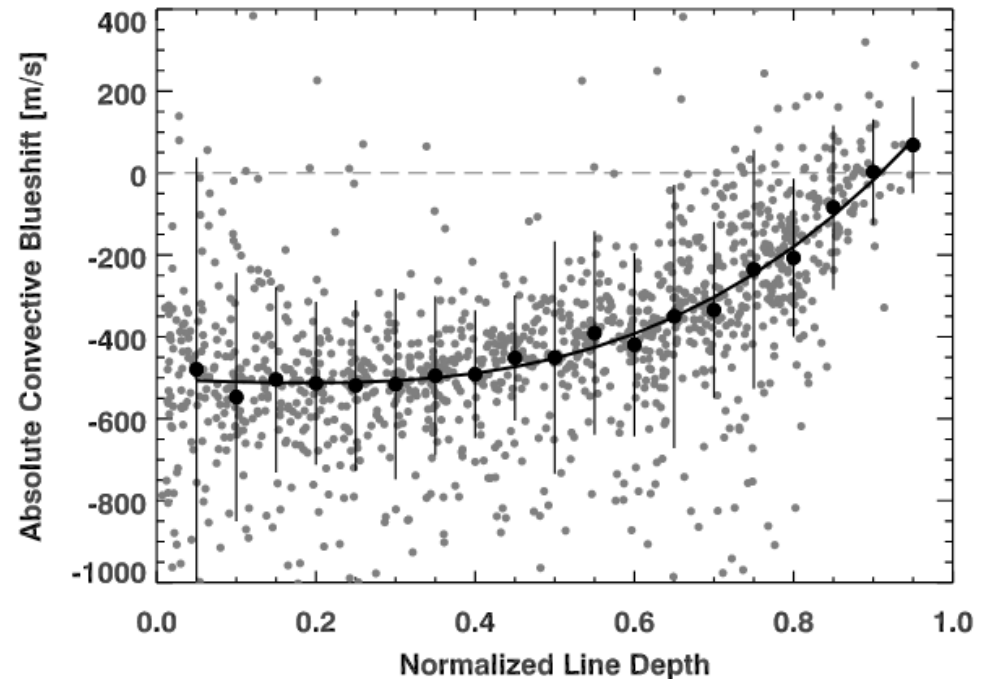


Figure 4: Granulation pattern for the Solar Flux Atlas.  
Imagen taken from [2].

---

[2] A. Reiners, N. Mrotzek, U. Lemke, J. Hinrichs, and K. Reinsch, The IAG solar flux atlas: Accurate wavelengths and absolute convective blueshift in standard solar spectra, *A&A* 587, A65 (2016).

# THE IMPORTANCE OF THE SOLAR GRANULATION PATTERN

Gray showed that Absolute shifts of spectral-line bisectors (the third signature of granulation) are shown to follow the solar pattern. The scale factors increase with effective temperature and are larger in giants than in dwarfs. [4].

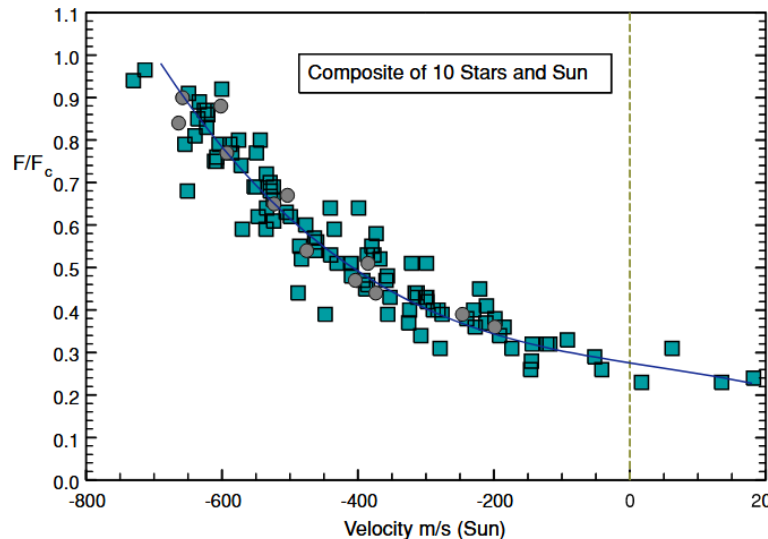


Figure 5: This composite of 10 stars (squares) delineates the universal third-signature plot for the core portion of the bisectors. The circles denote the solar lines. The velocity scale is for the solar case. Imagen taken from [4]

---

[4] D. F. Gray, THE THIRD SIGNATURE OF STELLAR GRANULATION, ApJ 697, 1032 (2009).

# WHAT IS THE CONVECTIVE BLUESHIFT FROM THE SUN?

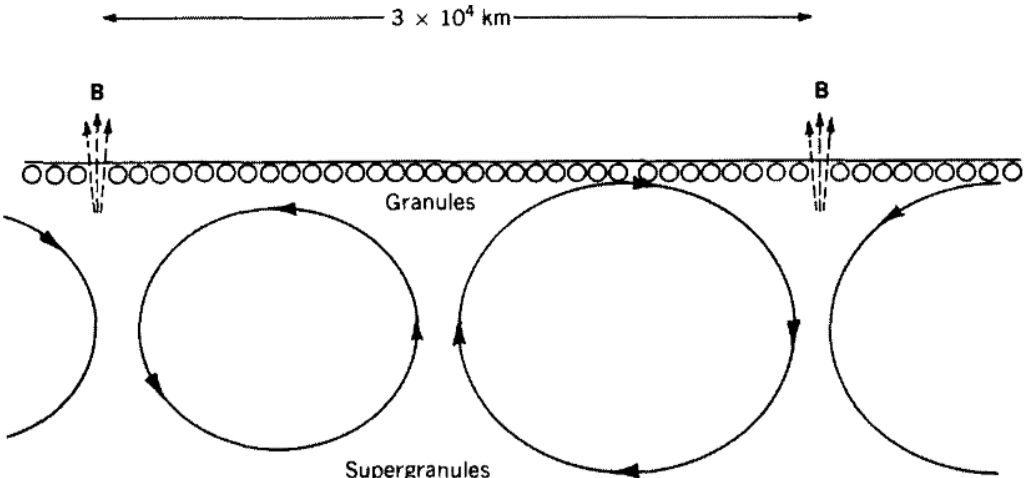


Fig. 5-10 Illustration of the approximate horizontal and vertical scales of granules and supergranules.

Figure 6: Convective movement in the sun. Imagen taken from [5].

- \* The Convective Blueshift is a direct consequence of convective motion in the Sun's outer layers.
- \* Fluid movements caused by density variations from temperature fluctuations in the Sun's outermost layer modify the spectrum, causing each spectral line to display distinct relative velocities.

---

[5] F. Peter, Solar Astrophysics. Cambridge research and instrumentation, 1990

When the Sun pushes material up through its outer layer, the spectrum exhibits a blueshift. As this material subsequently cools and falls back through the atmosphere, it produces a redshift, but emits less light, making the blueshift dominant [5].

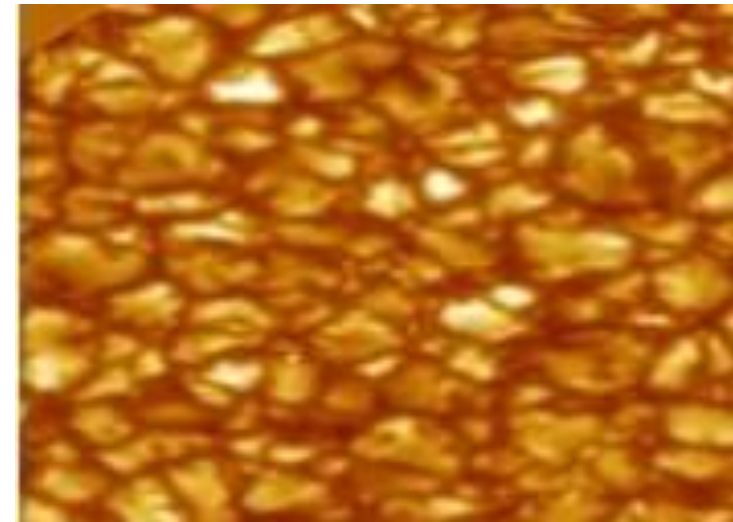


Figure 7: Diagram of convective blueshift, showing why blueshift is the dominant effect. Imagen adapted from [1].

---

[1] S. A. Hamouda, F. F. Alfarjani, and F. Y. Elfituri, “Sunspots production and relation to other phenomena: A review”, International Journal of Science and Research Methodology (2018).

[5] F. Peter, Solar Astrophysics. Cambridge research and instrumentation, 1990

# ASYMMETRIES DUE TO THE CONVECTION MOVEMENT

To accurately measure velocities, we must account for the characteristic C-shaped bisector of spectral lines, which is a direct result of this convection.

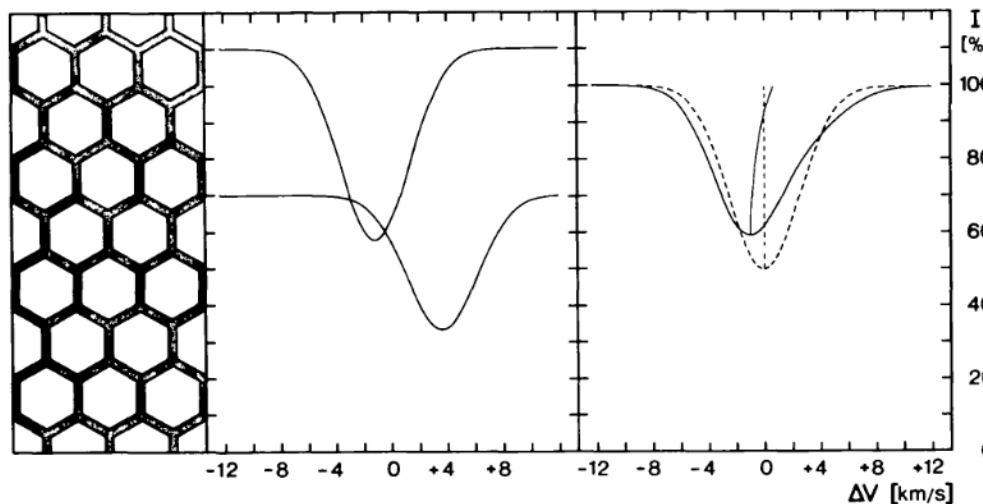


Figure 8: Origin of spectral line asymmetries and wavelength shifts caused by convection. Left: Idealized White-light image of solar granulation. Center: Spectral line profiles observed under high spatial resolution. Right: Solid curve gives the resulting profile for observations under low spatial resolution [6].

---

[6] D. Dravins, L. Lindegren, and A. Nordlund, Solar granulation - Influence of convection on spectral line asymmetries and wavelength shifts, *Astronomy and Astrophysics* 96, 345 (1981).

# METHODOLOGY

- \* This project started with the work of Professor Benjamin and Manuel Fuentes. Their analysis of the visible range in the Solar Flux Atlas revealed a clear chromodependence within the granulation pattern.
- \* We continue with a characterization of solar dynamics and line asymmetries based on granulation pattern observations.
- \* We follow the methodology established in previous studies [3,6,7] , which utilized a selected list of Fe I lines. These lines are ideal for this calibration due to their minimal thermal broadening and reduced susceptibility to other atmospheric affectations..

---

[3] M. Ellwarth, B. Ehmann, S. Schäfer, and A. Reiners, Convective characteristics of Fe I lines across the solar disc, *A&A* 680, A62 (2023).

[6] D. Dravins, L. Lindegren, and A. Nordlund, Solar granulation - Influence of convection on spectral line asymmetries and wavelength shifts, *Astronomy and Astrophysics* 96, 345 (1981).

[7] D. F. Gray and B. Oostra, The Solar-flux Third Granulation Signature, *The Astrophysical Journal* 852, 42 (2018).

# NAVE BLEND-FREE LIST OF FE I LINES

- \* The previous methodology implemented the Nave et. al list of laboratory measured Fe I lines [8]. This list classifies lines with a quality rating (A,B,C,D).
- \* Not all the listed lines are clearly present in the solar spectrum, and within the near-infrared range, many lines are severely mixed.
- \* In collaboration with Professor Benjamin and Manuel Fuentes, we refined this list. First, we selected only quality A lines and then performed a visual inspection to discard line mixes or absent from the solar spectrum.
- \* The new blend-free list improves our results, leading to cleaner graphics and characterization with less scatter in the data.

---

[8] G. Nave, S. Johansson, R. C. M. Learner, A. P. Thorne, and J. W. Brault, A New Multiplet Table for Fe i, *The Astrophysical Journal Supplement Series* 94, 221 (1994).

Line up for the code:

1. Identify the Fe I lines in the IAG Solar Flux Atlas and the IAG Spatially Resolved Quiet Sun Atlas using the blend-free list of Fe I lines.
2. Fit a fourth-grade polynomial fit due to the c-curved line profile bisector and find the observed wavelength.
3. Calculate the Doppler velocity, convective blueshift and flux with the fit.
4. Find the second derivate and the third derivate relation for the curvature in the observed wavelength.

Second derivate evaluated in the observed wavelength

$$\frac{d^2 p(\lambda)}{d\lambda^2} \lambda^2$$

Core curvature

Third derivate relation evaluated in the observed wavelength

$$-\frac{\frac{d^3 p(\lambda)}{d\lambda^3}}{3 \left( \frac{d^2 p(\lambda)}{d\lambda^2} \right)^2} \frac{c}{\lambda}$$

Bisector slope

# WHAT WE FOUND

Our results can be summarized by 3 principal aspects:

- \* Chromodependence on the granulation pattern along the line depth.
- \* A detailed view of the characteristic curvature, asymmetries, and sharpness of spectral lines.
- \* Higher-quality graphs with reduced scatter.

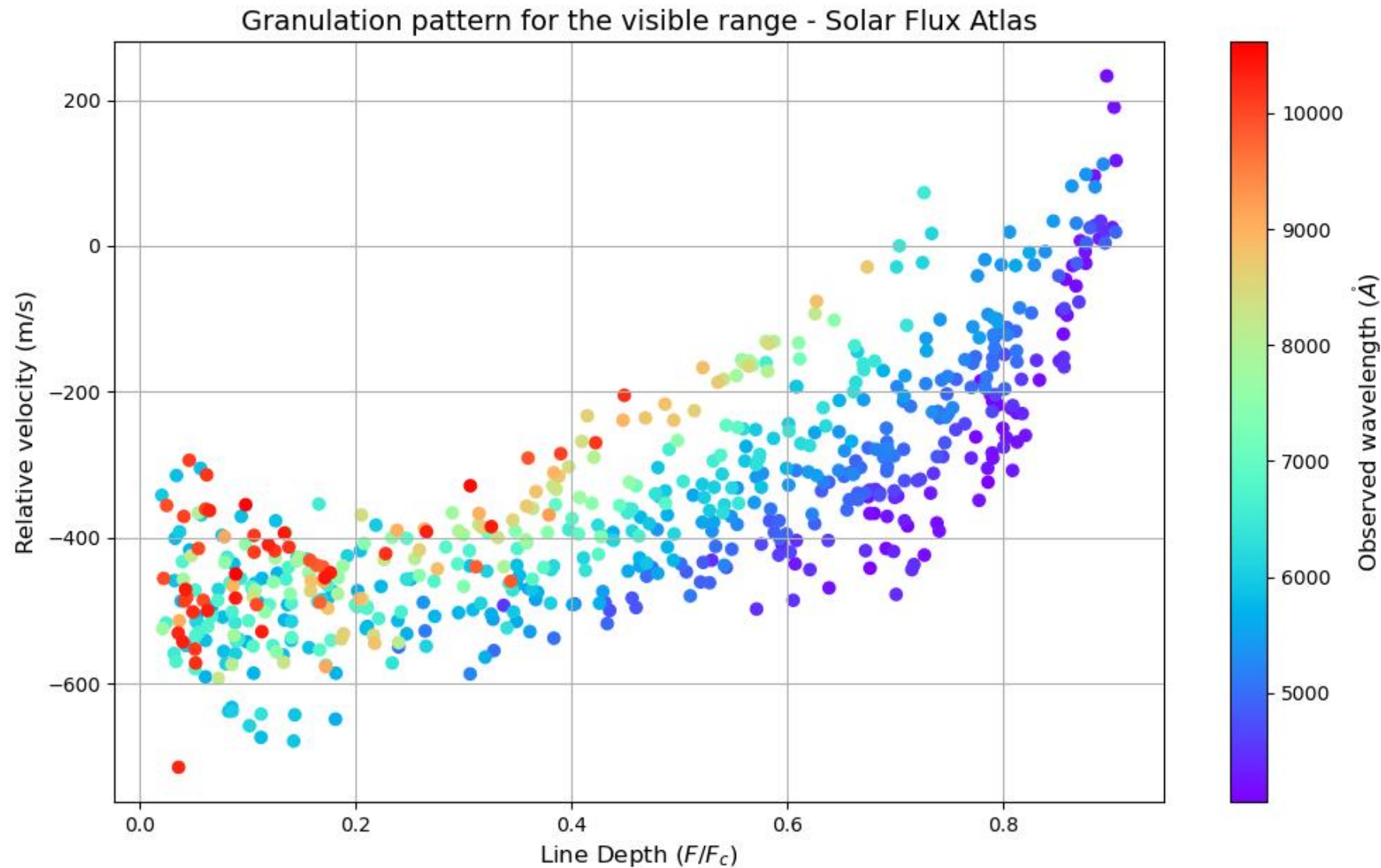


Figure 9: Granulation pattern for the visible range in the Solar Flux Atlas. The chromodependence along line depth effect is clearly visible.

### Granulation pattern for the visible range - Spatially Resolved Atlas

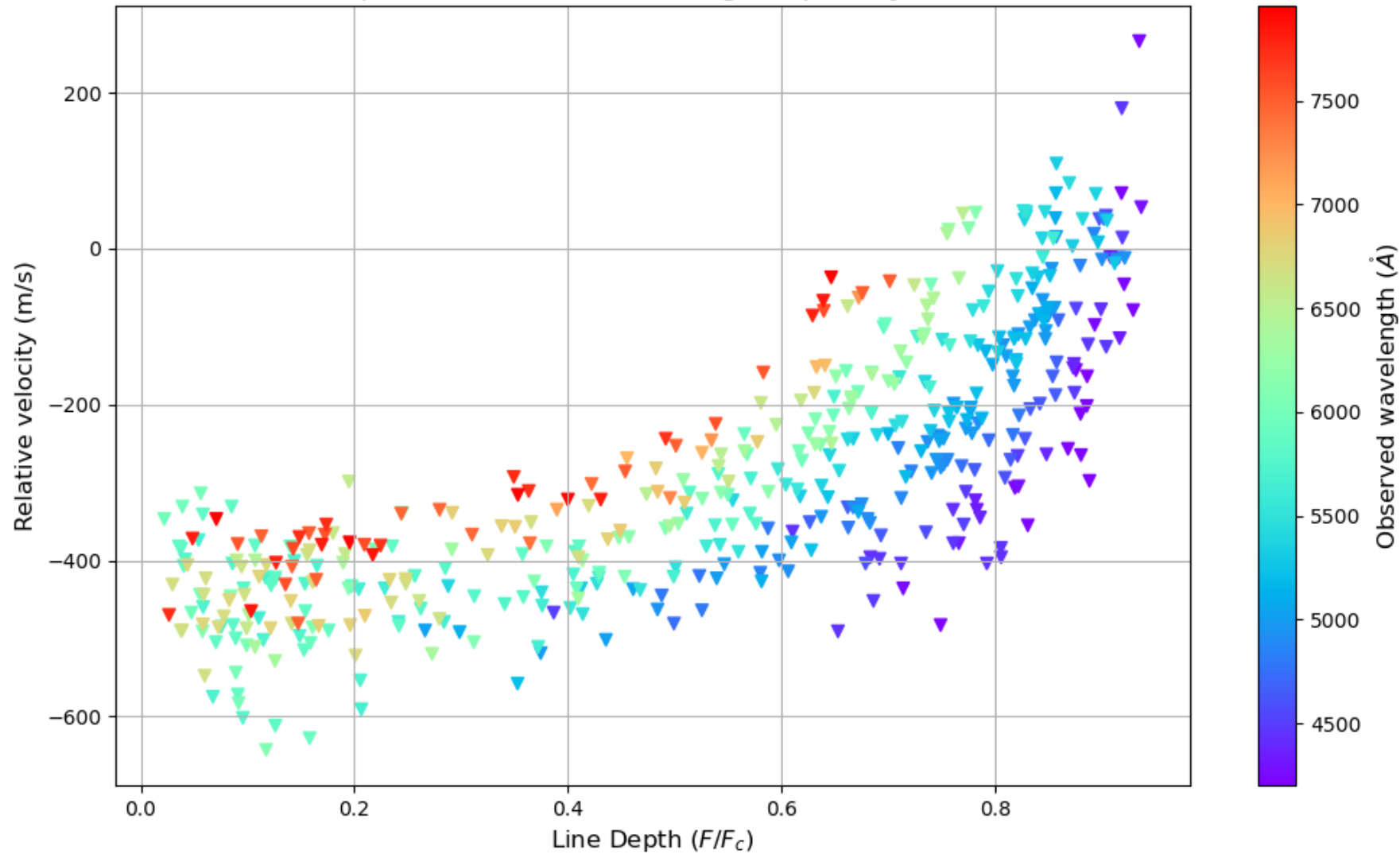


Figure 10: Granulation pattern for the visible range in the Spatially Resolved Quiet Sun Atlas. The chromodependence along line depth effect is clearly visible.

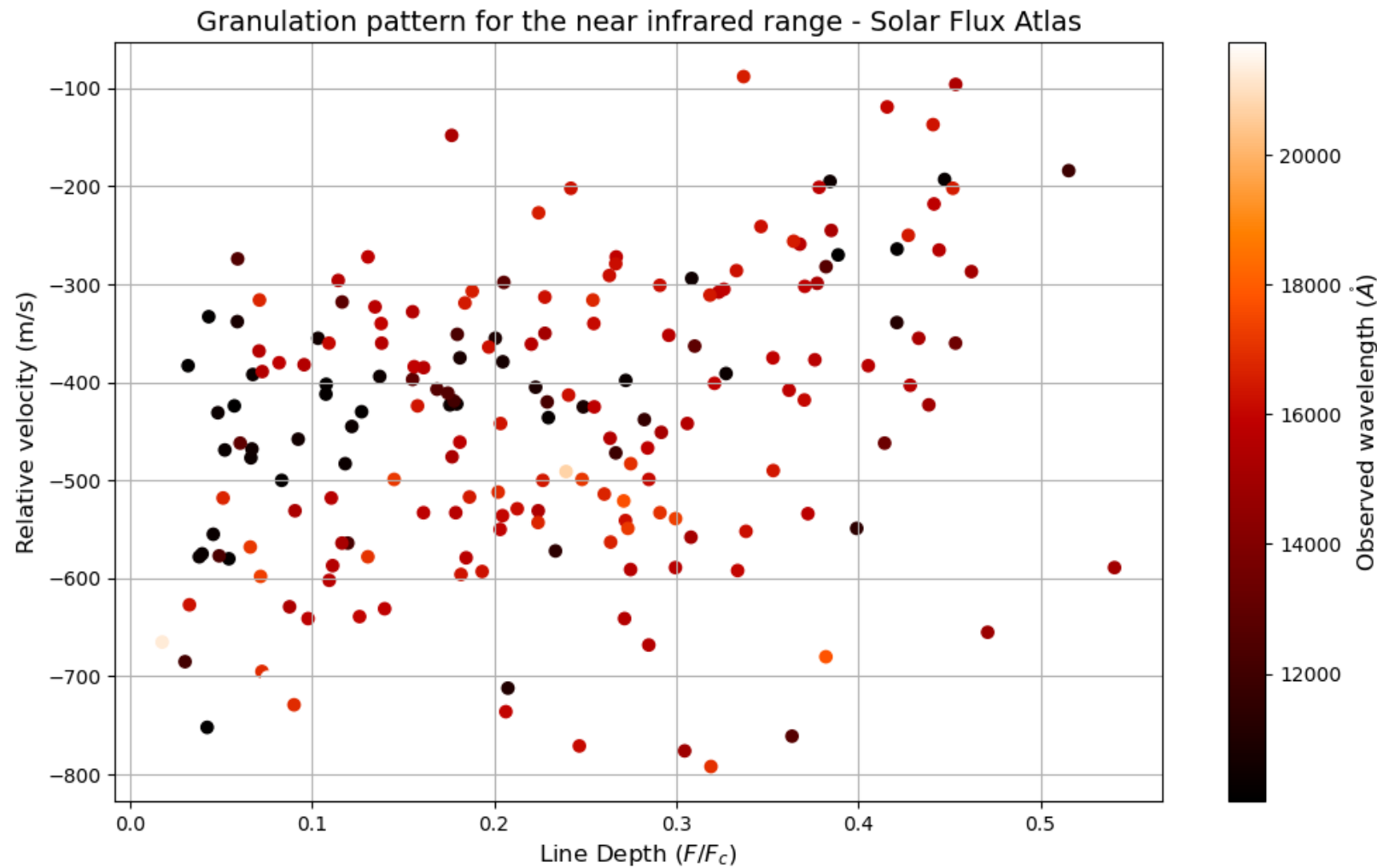


Figure 11: Granulation pattern for the near infrared range in the Solar Flux Atlas.

# CHARACTERIZATION OF CHROMODEPENDENCE

Our initial approach was to follow the methodology of Gray & Oostra [7], which describes the granulation pattern using a standard second-order polynomial fit.

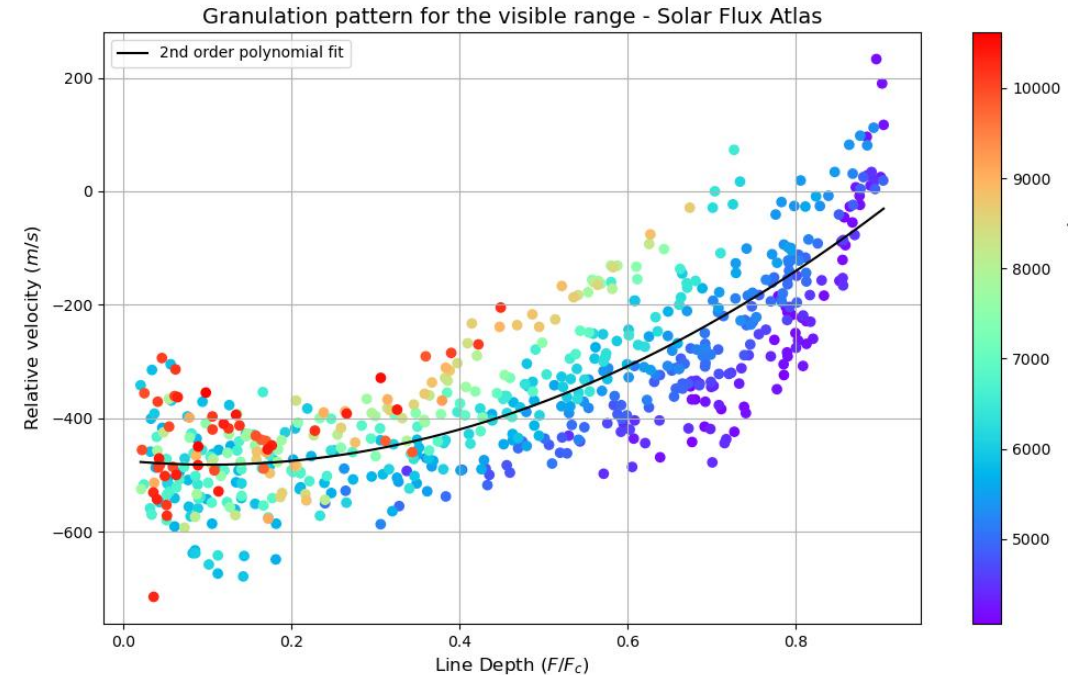


Figure 12: Granulation pattern for the visible range in the Solar Flux Atlas. The black line represents the standard second-order polynomial fit.

However, our goal is to obtain a curve that describes the chromodependence.

---

[7] D. F. Gray and B. Oostra, The Solar-flux Third Granulation Signature, The Astrophysical Journal 852, 42 (2018).

The second approach was establishing different second order polynomial fit curves for each color range. We see that the effect of chromodependence is pronounced just for the ultraviolet range on the two types of spectral data.

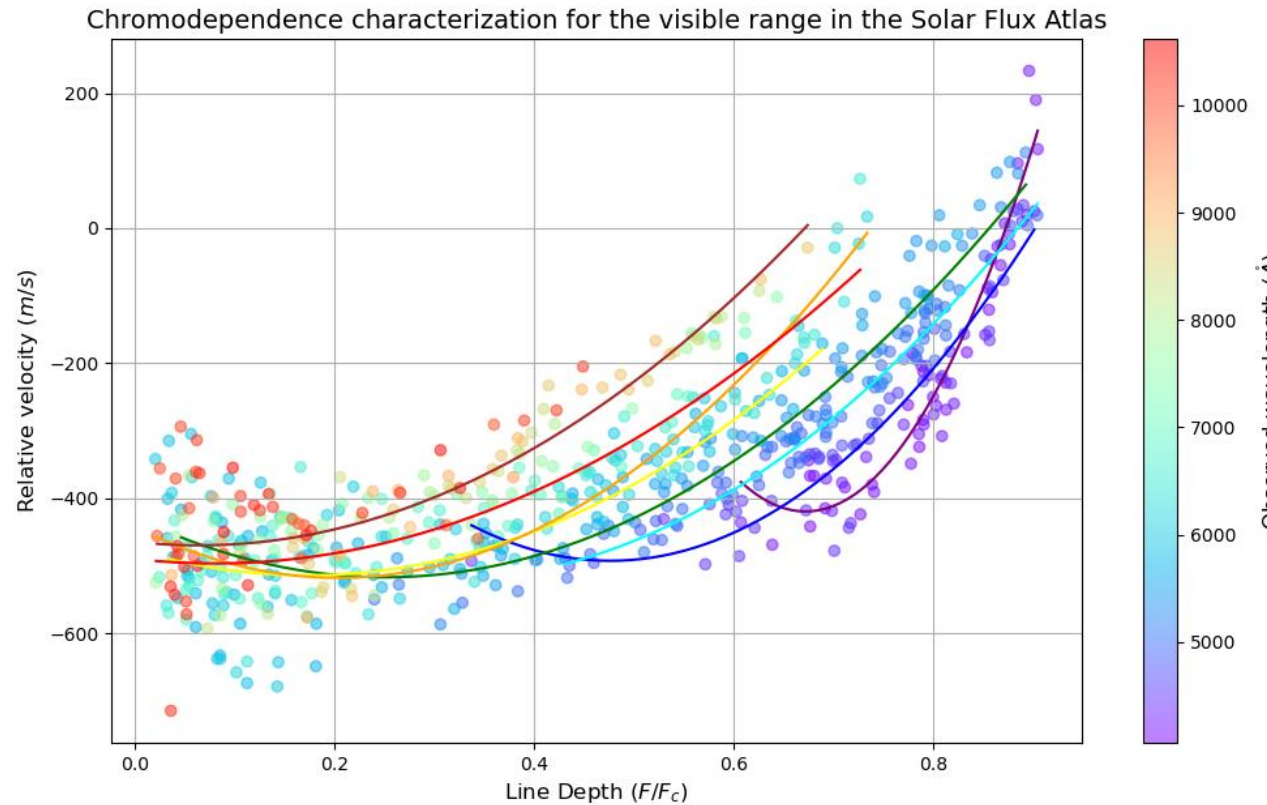


Figure 13: Granulation pattern for the visible range in the Solar Flux Atlas. The different second order polynomial fit curves for each color range are shown.

On the way toward a generalized characterization, we graphed the coefficients, which reveal a rational trend with a significant increase in the violet range.

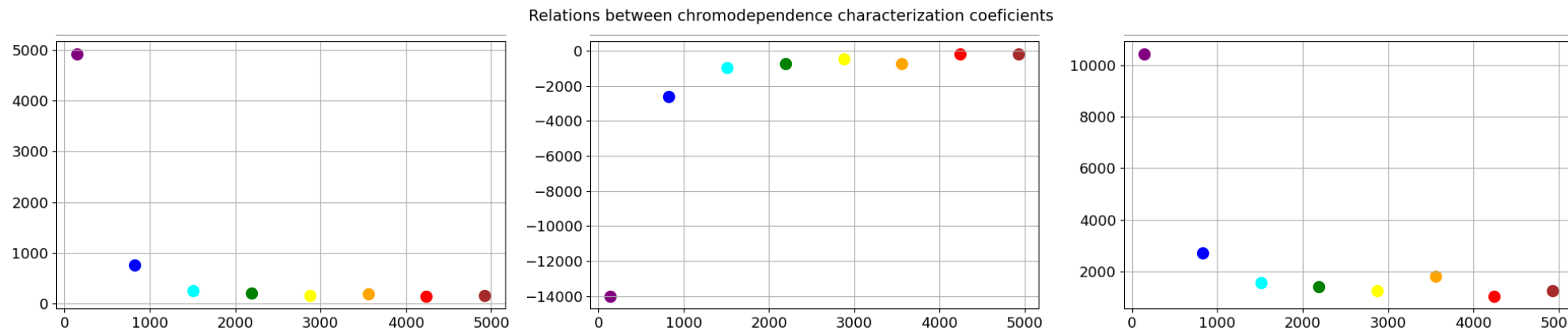


Figure 14: Different coefficients for the color-curves in the granulation pattern. They reveal a rational trend with a significant increase in the violet range.

We are still working on the coefficients, but to find a solution, we must describe the problem.

- \* We performed an analysis of line depth against wavelength. Our hypothesis was:  
“If the chromodependence is present only in the Solar Flux Atlas, then rotation could be the cause of this phenomenon”
- \* We observed a chromodependence in both spectral datasets. This was initially unexpected because the rotation is negligible at the disc center.
- \* We took a 4300-5600 Å range and sorted all lines from both atlases into 50 m/s velocity bins.

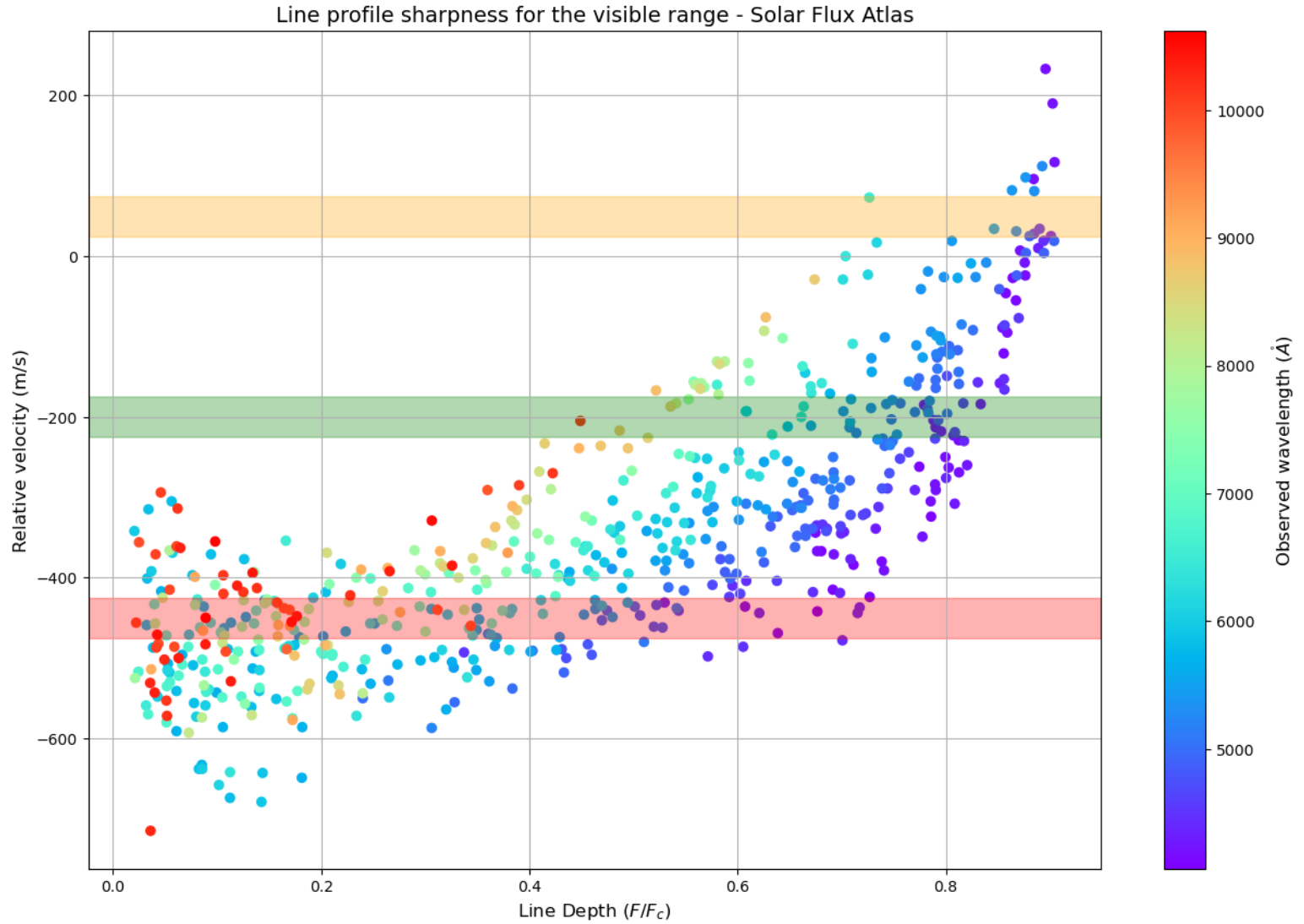
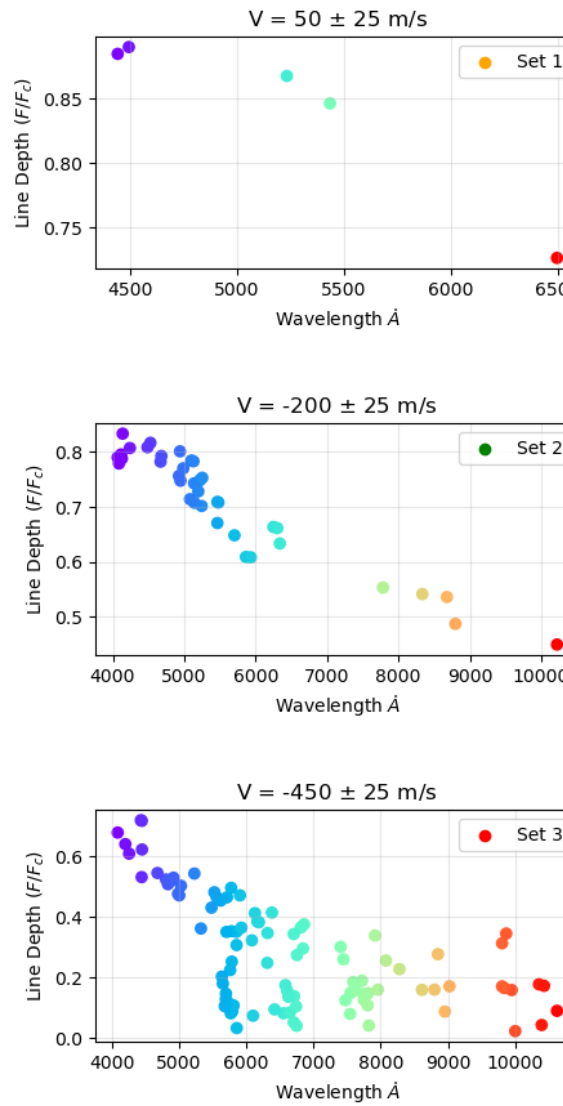


Figure 15: Example of selected velocity bins used for the analysis in the Solar Flux Atlas. Each panel corresponds to a different radial velocity range, showing the spectral line behavior within that bin.

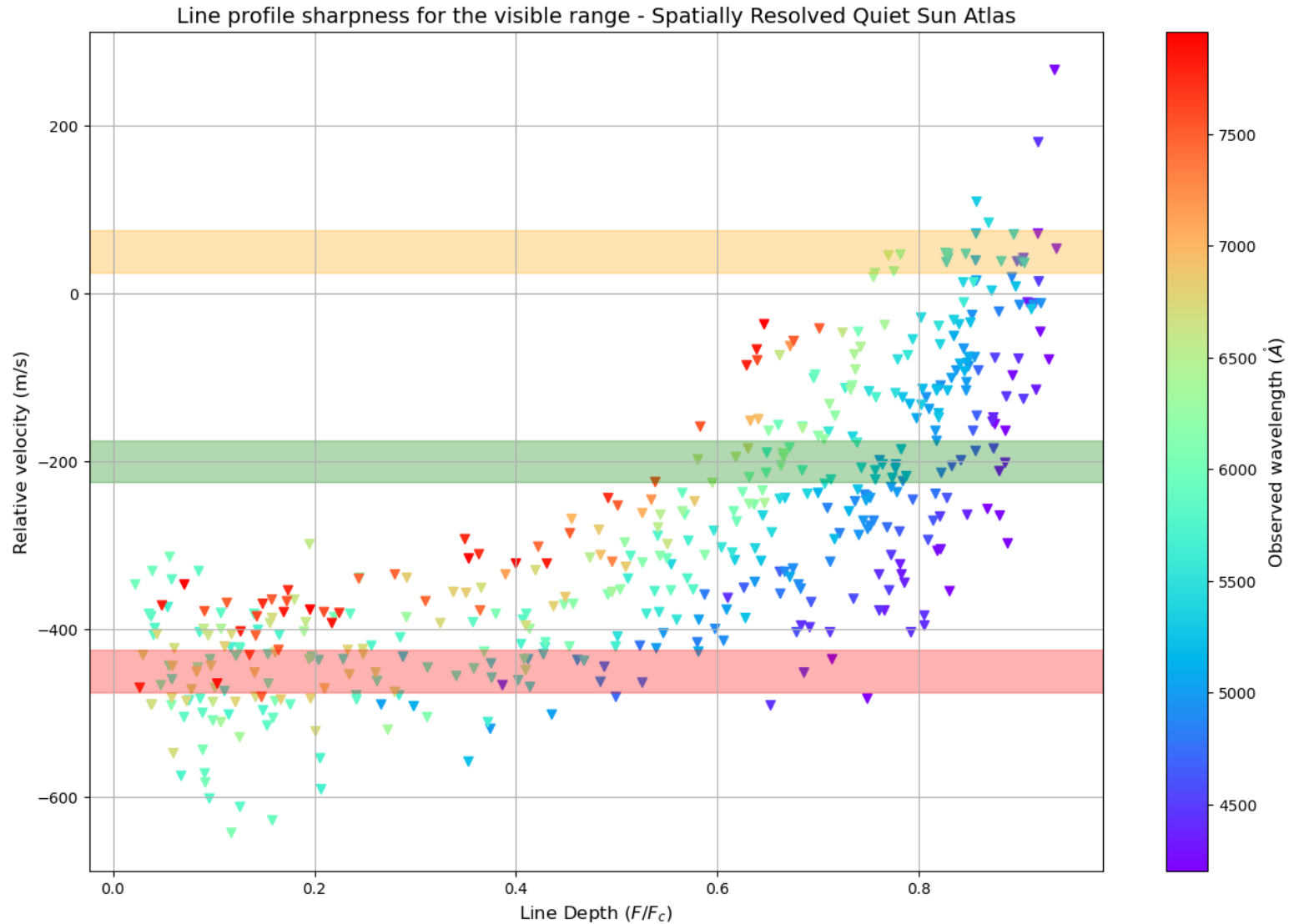
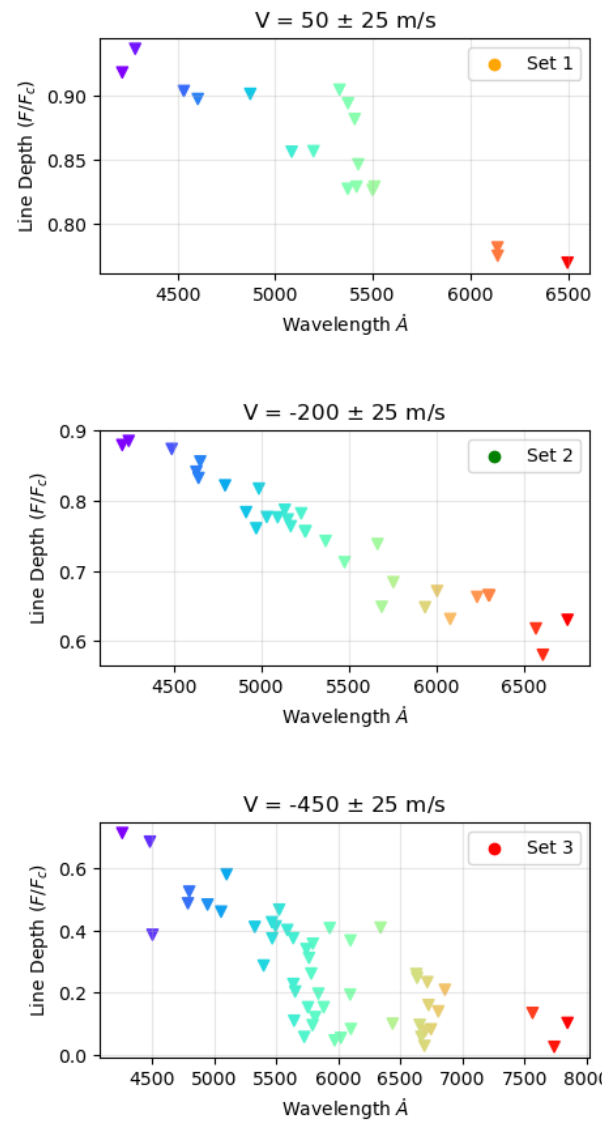
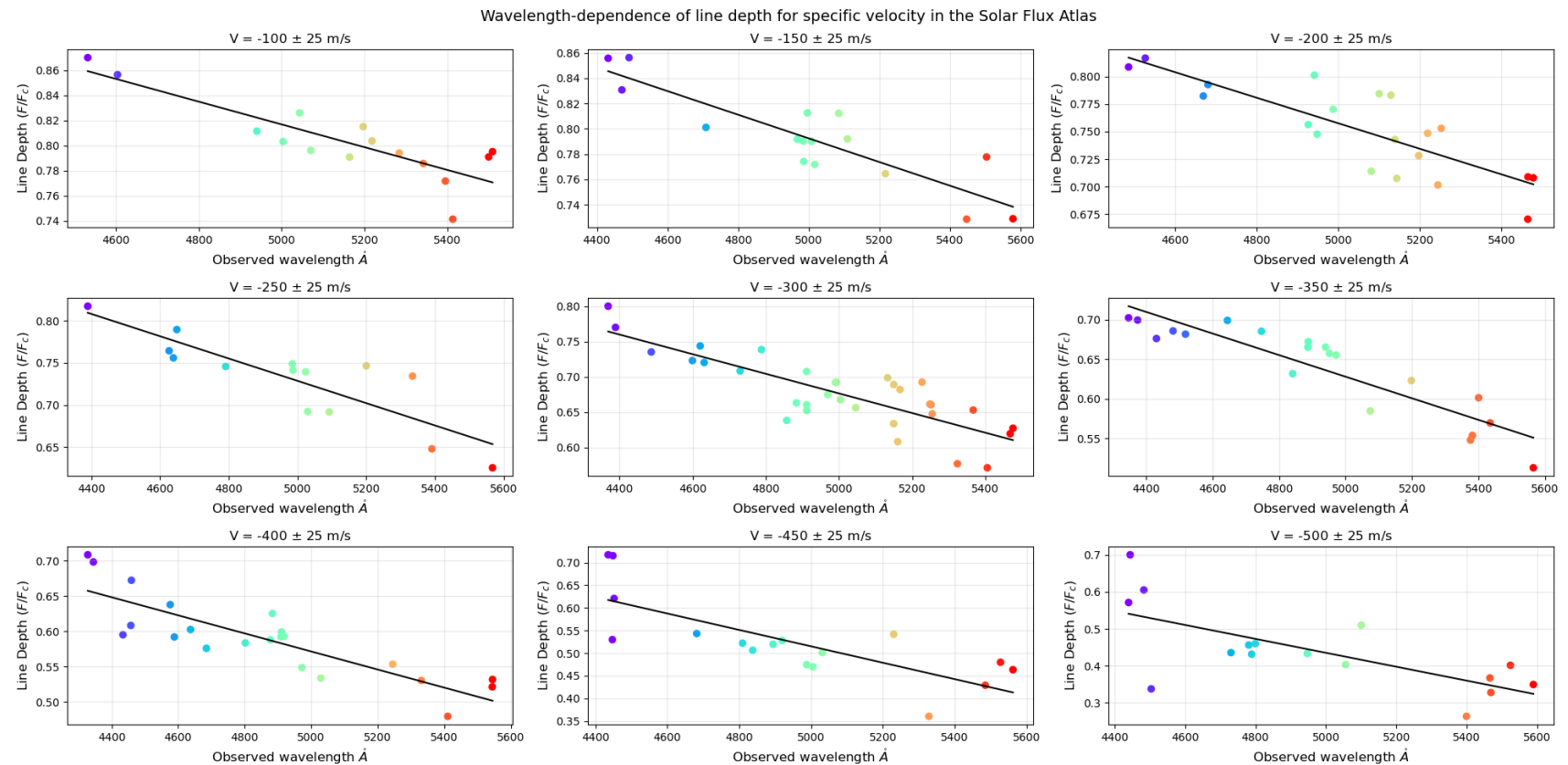
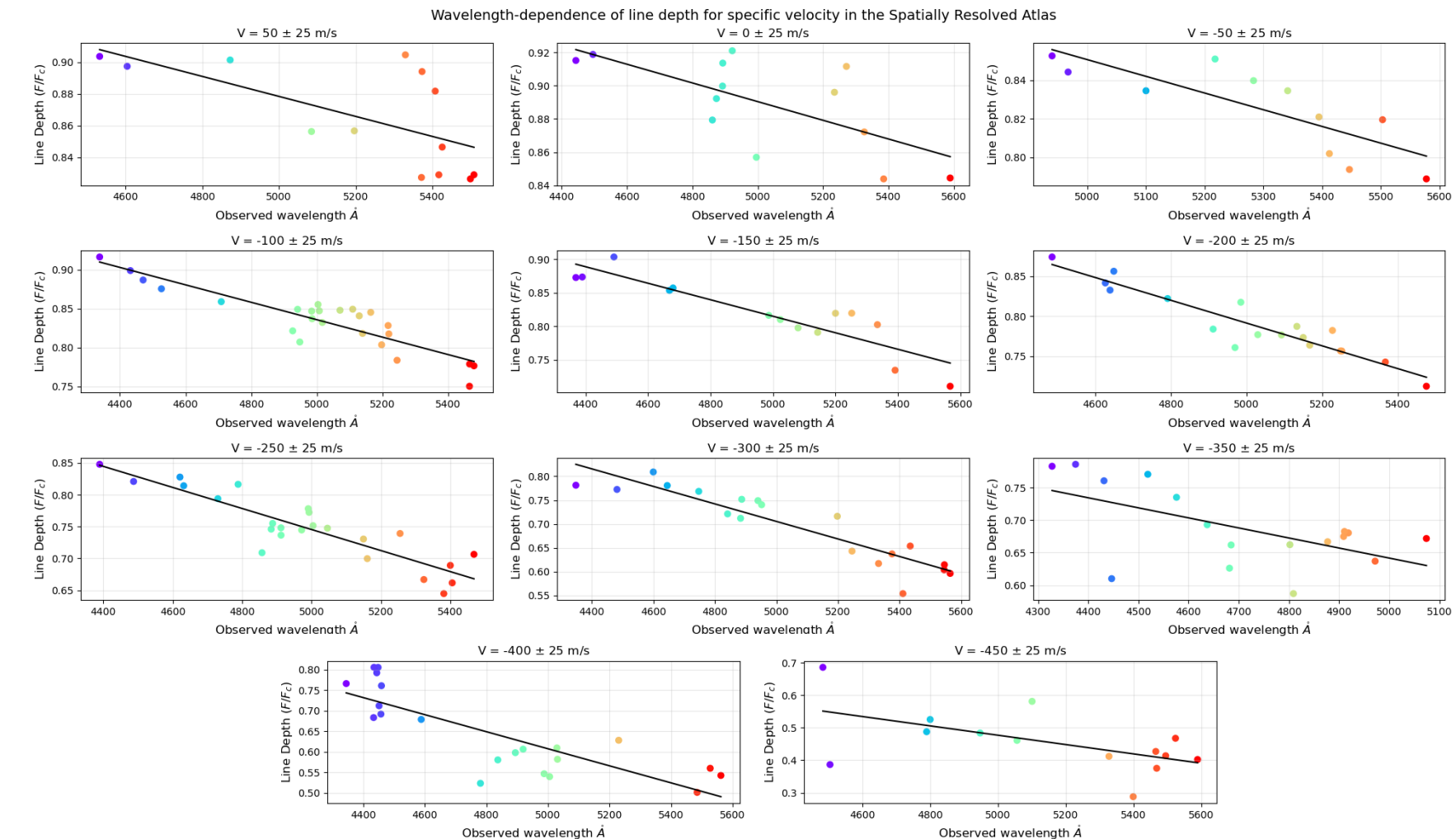


Figure 16: Example of selected velocity bins used for the analysis in the Spatially Resolved Quiet Sun Atlas. Each panel corresponds to a different radial velocity range, showing the spectral line behavior within that bin.



Velocity	Slope	Intercept
-100	1.270	-0.000091
-150	1.260	-0.000094
-200	1.337	-0.000116
-250	1.392	-0.000133
-300	1.372	-0.000139
-350	1.310	-0.000137
-400	1.211	-0.000128
-450	1.421	-0.000181
-500	1.378	-0.000189

Figure 17: The figure shows line depth as a function of wavelength, categorized by velocity bin. Each data series was fitted with a linear polynomial function; the corresponding slopes of these fits are presented in the table for the Solar Flux Atlas.



Velocity	Slope	Intercept
50	1.193	-0.000063
0	1.172	-0.000056
-50	1.284	-0.000087
-100	1.395	-0.000112
-150	1.432	-0.000124
-200	1.502	-0.000142
-250	1.571	-0.000165
-300	1.623	-0.000184
-350	1.412	-0.000154
-400	1.645	-0.000208
-450	1.195	-0.000144

Figure 18: The figure shows line depth as a function of wavelength, categorized by velocity bin. Each data series was fitted with a linear polynomial function; the corresponding slopes of these fits are presented in the table for the Spatially Resolved Quiet Sun Atlas.

# SHARPNESS

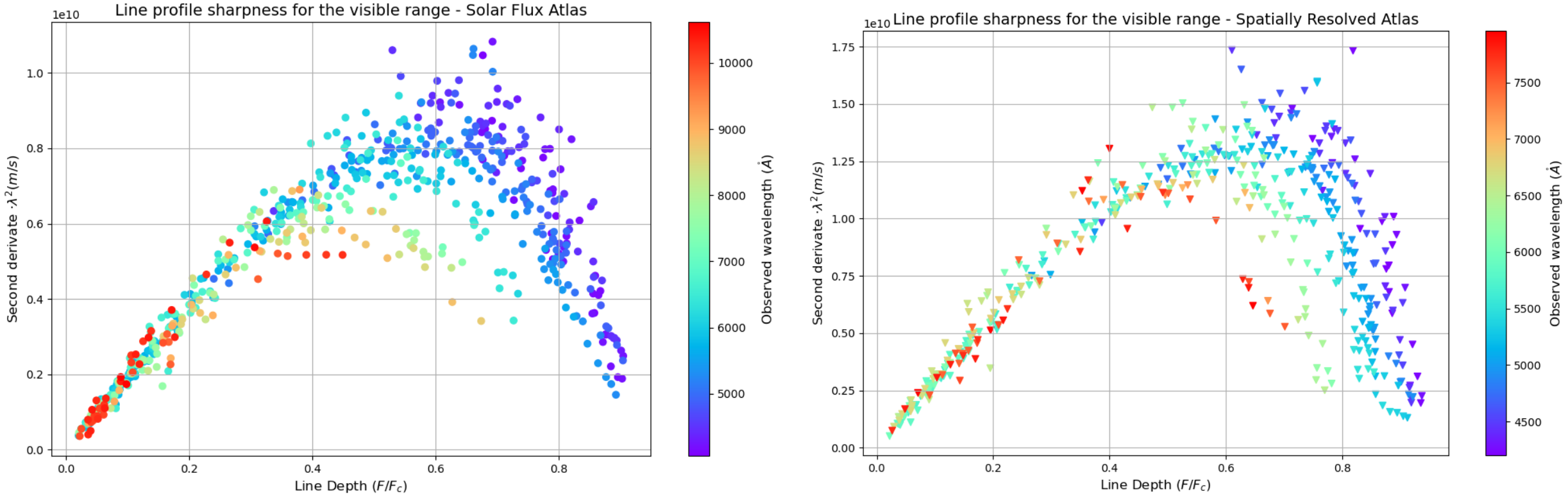


Figure 19: Sharpness of line profile for the visible range in both atlas.

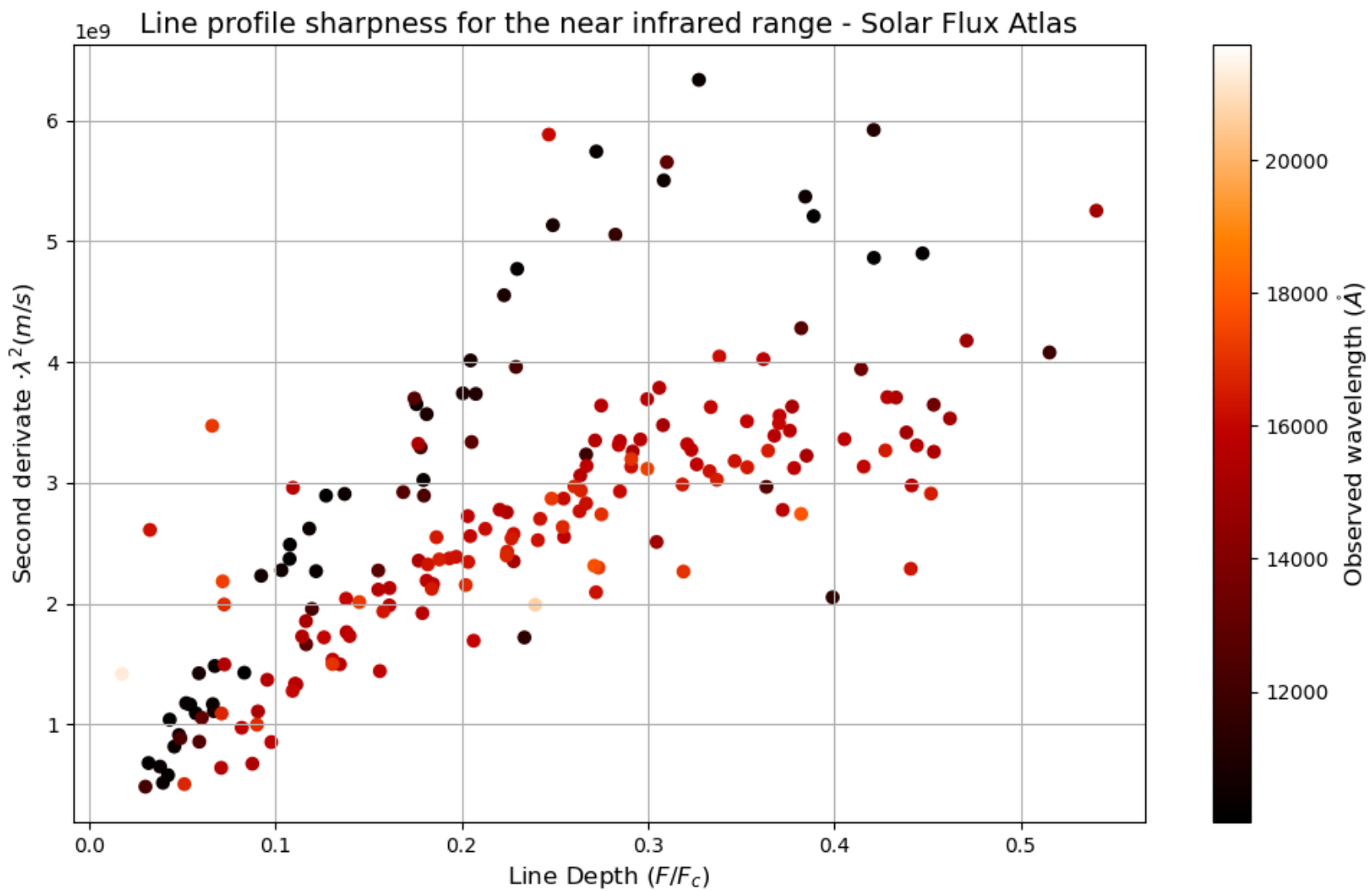


Figure 20: Sharpness of line profile for the near infrared range in the Solar Flux Atlas.

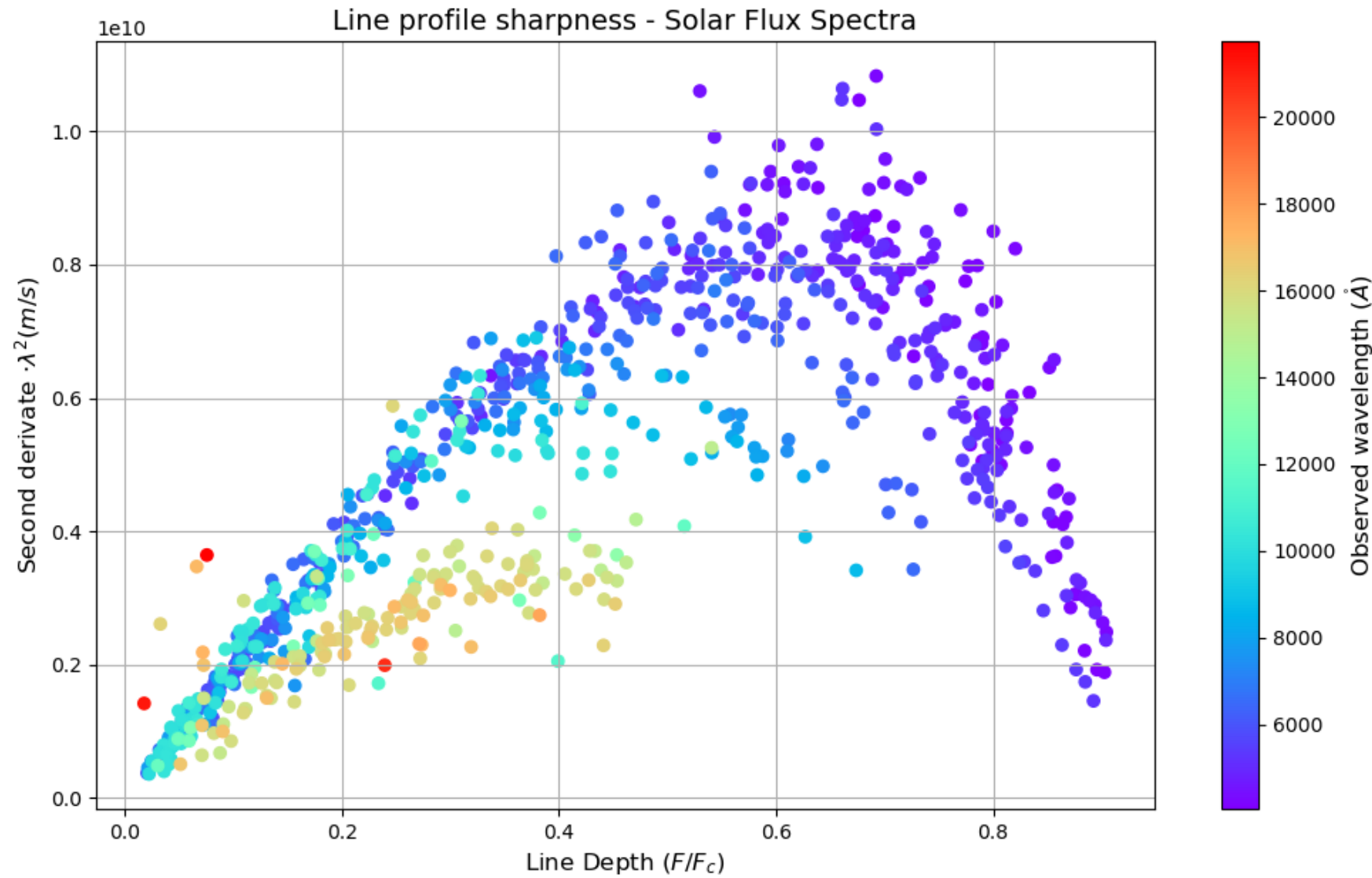


Figure 21: Graph for line profile sharpness in the Solar Flux Spectra.

# C-CURVED LINE PROFILE BISECTOR

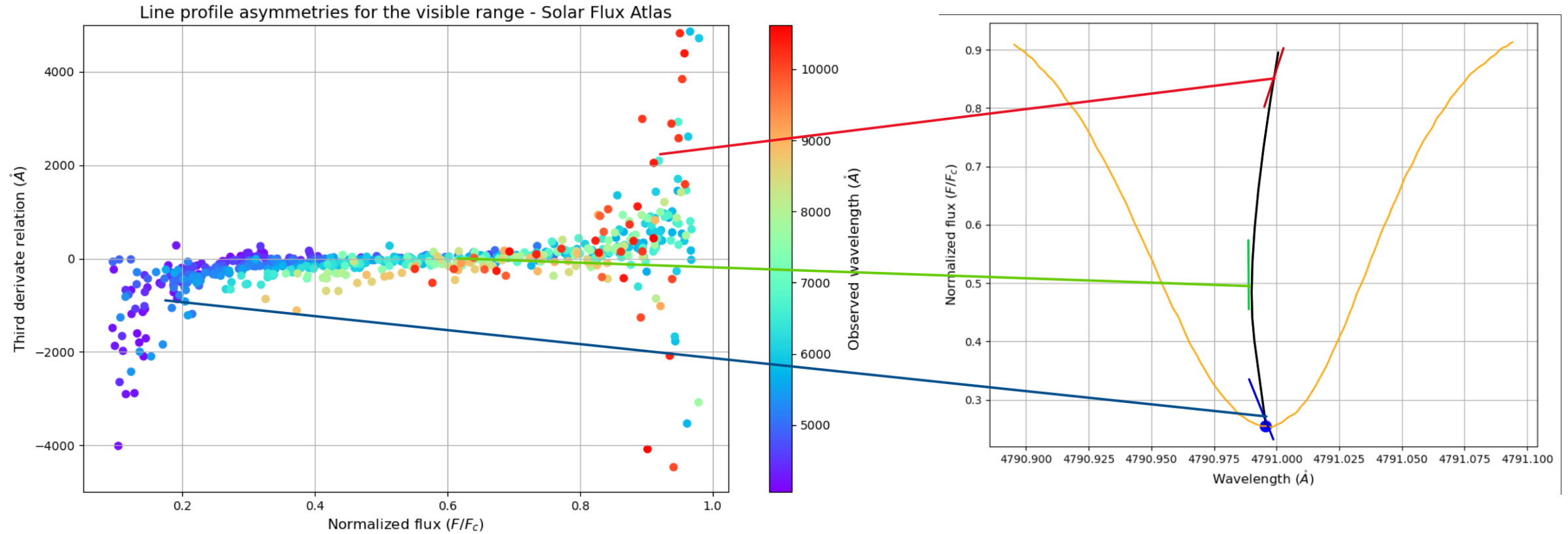


Figure 22: Plot of the c-curved line profile bisector behavior against line depth for the visible range in the Solar Flux Atlas.

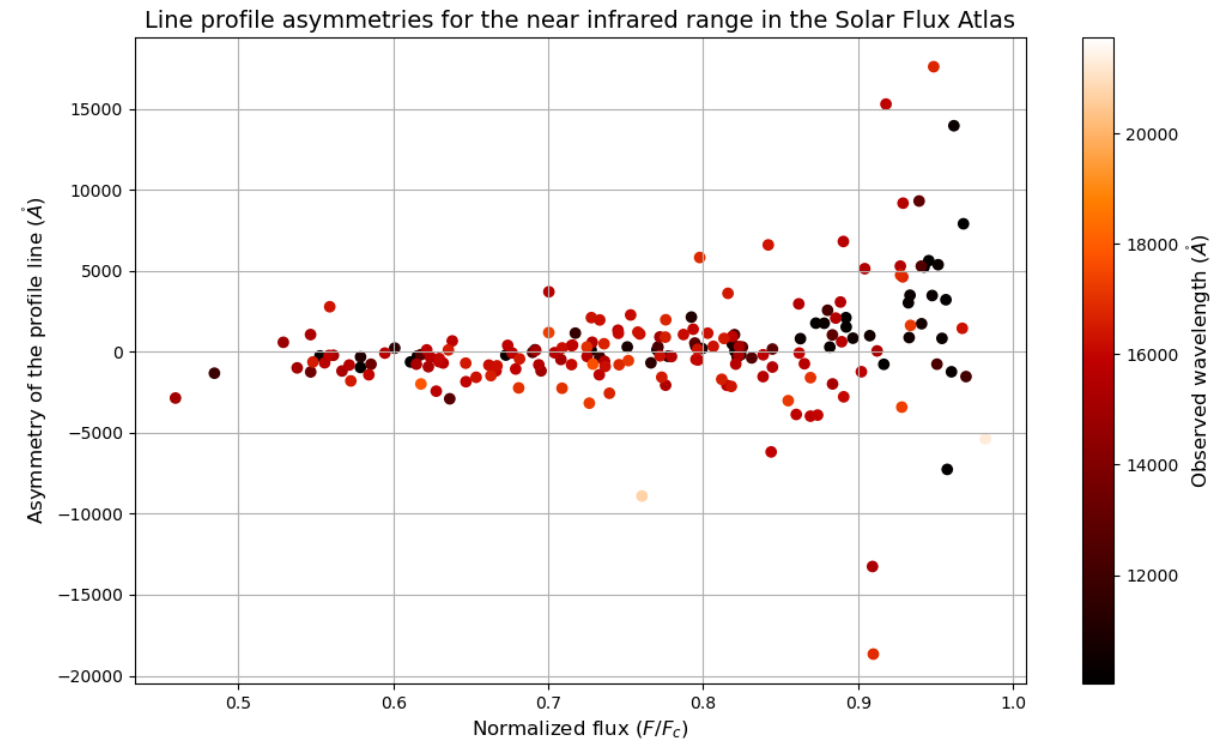
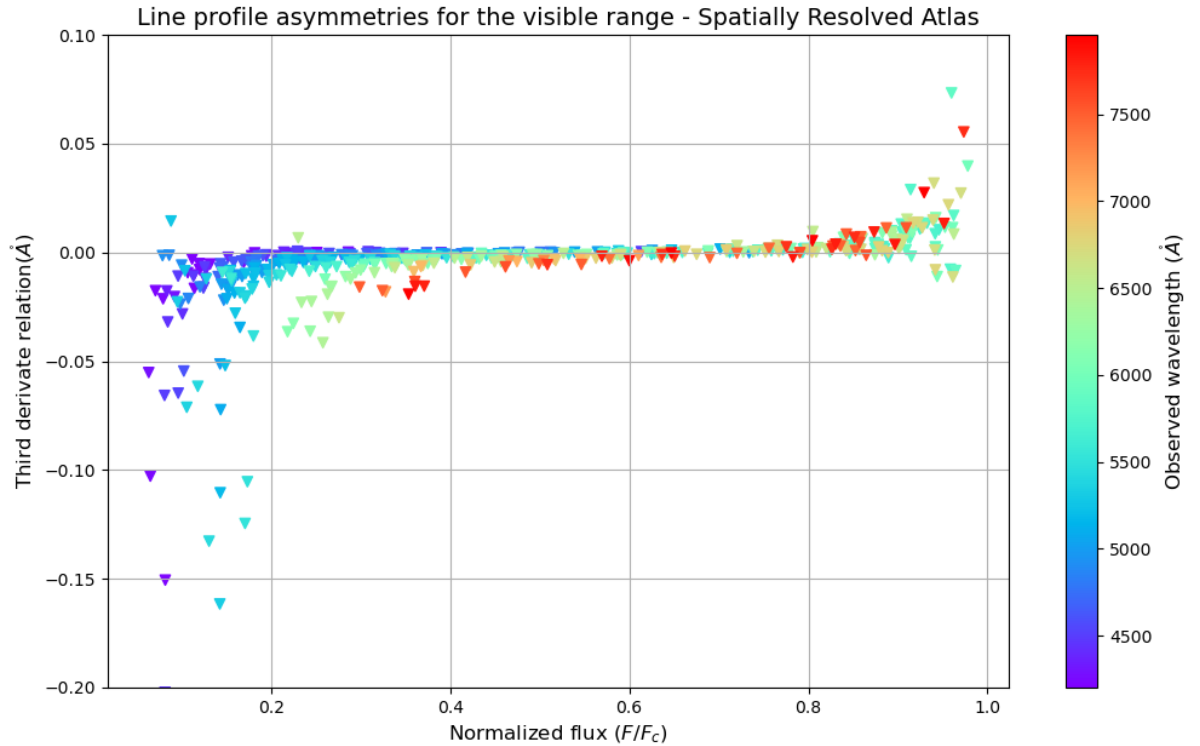


Figure 23: Plot of the c-curved line profile bisector behavior against line depth. Right: In the visible range in the Spatially Resolved Quiet Sun Atlas. Left: In the near infrared range in the Solar Flux Atlas.

# LESS SCATTERED POINTS

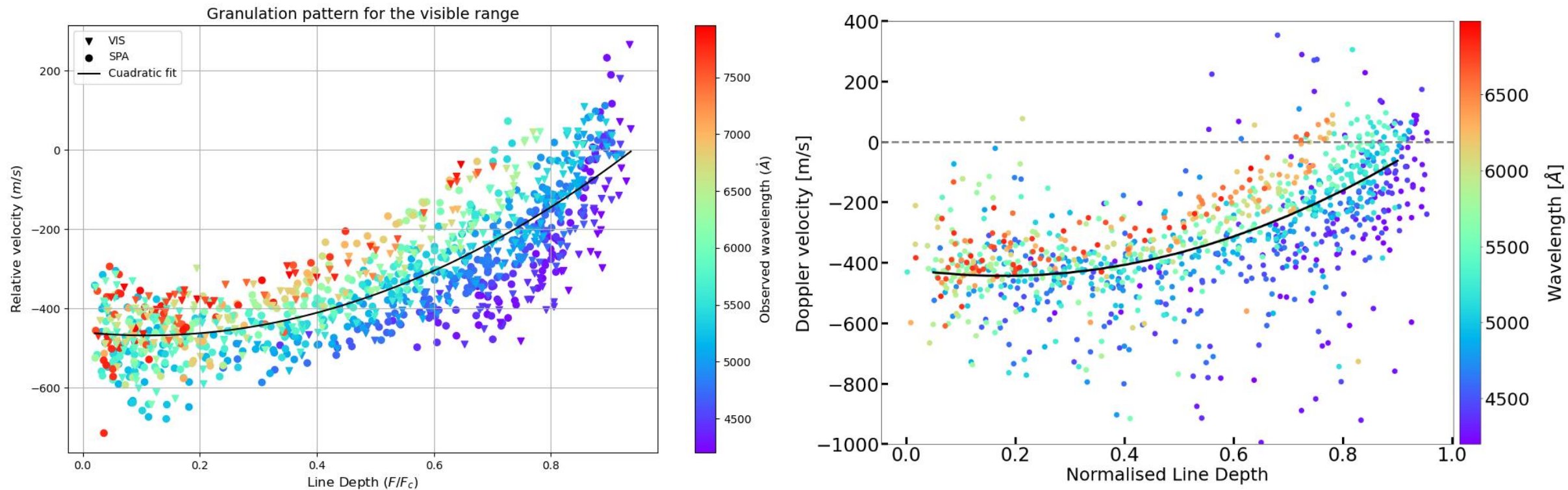


Figure 24: Comparison between the granulation patterns and Gray's standard curve in the visible range of the Solar Flux Atlas. Left: Granulation pattern with the Nave blend-free list of Fe I lines. Right: Granulation pattern with the Nave list of Fe I lines taken from [3]. A significantly reduced point scatter is evident.

[3] M. Ellwarth, B. Ehmann, S. Schäfer, and A. Reiners, Convective characteristics of Fe I lines across the solar disc, *A&A* 680, A62 (2023).

# PROGRESS

Characterize the convective blueshift of solar absorption lines and its dependence in line depth and wavelength range.

- Produce a blend-free list of Fe I absorption lines. (100%)
- Produce a solar granulation plot with minimal scatter. (100%)
- Describe in detail how the granulation plot depends on wavelength range. (80%)
- Explore possible explanations of wavelength-dependence.(30%)
- Explore ways of dealing with the wavelength-dependence when using the solar spectrum as a gauge for stellar spectra. (0%)